

Article

# New Design of an Electrical Excavator and Its Path Generation for Energy Saving and Obstacle Avoidance

Omid Ahmadi Khiyavi , Jaho Seo \*  and Xianke Lin 

Department of Automotive and Mechatronics Engineering, Ontario Tech University, Oshawa, ON L1G 0C5, Canada; omid.ahmadikhiyavi@ontariotechu.net (O.A.K.); xianke.lin@ontariotechu.ca (X.L.)

\* Correspondence: jaho.seo@ontariotechu.ca; Tel.: +1-905-721-8668 (ext. 7341)

**Abstract:** This study's goals are divided into two categories. The first is to design and build an excavator equipped with parallel electrical linear actuators. The second is to generate and test a PSO-based and a PFM-based path for this excavator in order to save energy by reducing energy consumption, improve the digging accuracy by minimizing the deviation between the desired and dug surfaces of the ground, and prevent colliding with subsurface objects. For this purpose, computer vision was employed to improve monitoring and verification. Five types of experiments were carried out in this investigation. The first two and the other three examined the impact of energy conservation in PSO- and PFM-based path generation, respectively. Finally, the results from these experiments were compared to identify and show the effect of optimal path generation.

**Keywords:** electrical excavator; motion and path planning; energy and environment-aware automation; collision avoidance; mechanism design



**Citation:** Ahmadi Khiyavi, O.; Seo, J.; Lin, X. New Design of an Electrical Excavator and Its Path Generation for Energy Saving and Obstacle Avoidance. *Vehicles* **2024**, *6*, 832–849. <https://doi.org/10.3390/vehicles6020040>

Academic Editor: Mohammed Chadli

Received: 12 April 2024

Revised: 7 May 2024

Accepted: 7 May 2024

Published: 9 May 2024



**Copyright:** © 2024 by the authors. Licensee MDPI, Basel, Switzerland. This article is an open access article distributed under the terms and conditions of the Creative Commons Attribution (CC BY) license (<https://creativecommons.org/licenses/by/4.0/>).

## 1. Introduction

One of the most important machines in the mining and construction sectors is the excavator. However, its operation labor cost is expensive, and there are possible hazards to the operator's life, particularly in mines. An autonomous excavator can provide a solution to this challenge. Additionally, operators of non-autonomous excavators must rest in the middle of their shifts, take a lunch break, and spend time while changing shifts. However, autonomous excavators are required to stop only when their energy supply runs out.

Hence, there is a necessity to devise algorithms aimed at reducing energy consumption in autonomous excavators, thereby extending their operational duration. Moreover, since these excavators are required to ensure precision in excavation and prevent collisions with underground obstacles in order to achieve autonomy, it is imperative to incorporate these considerations into the algorithms governing their digging motions.

Nowadays, fossil fuels provide the majority of the energy required by excavators. Because this form of energy source is harmful to the environment, it is vital to utilize electric machines more frequently than previously [1–4]. The hydraulic excavator, in particular, uses a significant amount of energy even while not in motion [5]. The hydraulic pump operates throughout idle working time to maintain the necessary liquid pressure. Furthermore, hoses and valves waste energy in hydraulic excavator systems [6], which has prompted researchers to apply electric linear actuators. These actuators are generally powered by electric motors and a series of ball screws (or lead screws) that need to withstand large axial stresses while consuming no energy when not in motion.

Numerous studies have explored the application of electric actuators in excavators. In [7], a novel mechatronic system utilizing DC motors and transistor power transducers was proposed for mining excavators, aiming to achieve a 20–30% reduction in power consumption. Additionally, in [8], researchers aimed to alleviate the load on electric actuators in excavators by incorporating an additional elastic damping device into the

excavator's kinematic scheme. Furthermore, Volvo introduced the EX02 [9], a fully electric excavator equipped with electric actuators to reduce noise pollution at construction sites.

The low back-drivability of electric actuators drew us to develop an electric excavator with this property [10]. However, when compared to hydraulic actuators, electric actuators may generate less force in general [11]. As a result, the excavators that employ these actuators should be designed differently such that the actuators bear lighter loads under the same external load on the bucket tip. The load capacity of the electric excavator may be increased with this design. Simultaneously, having a reduced load on the actuators reduces their energy consumption.

The path generation algorithm, in addition to modifying the excavator design, can help reduce energy consumption for autonomous excavation. Several studies have been conducted on excavation path generation for excavators. In [12], the researchers used an impedance control to avoid objects. This strategy can decrease energy consumption throughout the excavation process by decreasing the applied force for digging. Also, in [13], before excavating, the researchers identified the soil properties. In this manner, the identified material properties can be incorporated into the path and motion to be generated.

In [14], a minimum torque and time variable trajectory optimization technique was applied to autonomous excavators by taking soil–tool interactions into account. The approach addresses geometric, kinematic, and dynamical restrictions while considering the excavation path as a trajectory optimization problem. The authors of [15] attempted to take the jerky and slow operator commands and transform them into quick and optimal motions for autonomous excavators using splines, which can contribute to reducing energy consumption and minimizing jerky motions. Also, in [16], the researchers developed an ideal bucket-filling algorithm for self-driving excavators to estimate the amount of soil in the bucket based on nonlinear and complicated models. This method allows the digging sequence to be optimized and more energy to be conserved. In [17], the trajectory for an autonomous excavator was generated using a nonlinear model predictive controller. They tested this strategy and confirmed its effectiveness using an excavator for grading.

Optimization algorithms have been used for path generation to optimize parameters for reducing energy consumption or path error reduction. In [18], the ant colony optimization (ACO) approach was employed to create an ideal route that consumes less energy and provides more accuracy in digging. The particle swarm optimization (PSO) technique was used by the researchers in [19] to create a route for an autonomous mobile robot. A novel fitness function that meets the obstacle avoidance and optimal path traversal requirements was modeled in this work, in which the robot travels toward the particle with the best fitness values. The potential field method (PFM) has been used as another method for autonomous mobile robot path planning [20]. Also, in [21], the authors developed and tested an energy-saving strategy with PFM-based path planning that utilized optimum sequence selection on a six-degree-of-freedom robotic manipulator. The authors of [22] used the PFM to build another method to keep robots from heading toward a local minimum or dead end. The extra energy required to return from a local minimum or dead end can thus be conserved.

None of the mentioned studies have considered all three aspects—energy savings, object avoidance, and tracking errors—simultaneously. Specifically, the existing state-of-the-art studies have focused on just one or two of these factors independently, but have not comprehensively investigated the combination of all three factors for an autonomous excavator. In this work, two distinct PSO-based and PFM-based techniques for integrating these three components were created and compared. The PFM excels in real-time applications due to its simplicity, efficiency, and decentralized control, making it ideal for dynamic environments. By simulating attractive forces toward the goal and repulsive forces from obstacles, PFM enables smooth trajectory planning while dynamically avoiding obstacles. Its decentralized nature allows each agent to make autonomous decisions based on local information, fostering scalability and adaptability in multi-agent systems. Moreover, PFM exhibits robustness to noise and uncertainty, and its parameters can be easily tuned to

optimize performance for specific scenarios, while PSO generally requires a few parameters to be tuned, making it easy to implement and apply to different optimization problems. Finally, the capabilities of the PSO and the PFM algorithms in energy consumption reduction were tested using a designed test platform with electric linear actuators.

### 2. Design and Fabrication of an Electric Excavator

The excavator’s conventional design (Figure 1) includes three actuators connected in series. As a result, the actuators are subjected to a significantly high load from the ground.



Figure 1. The conventional CAT mini excavator [23].

The arm and bucket actuators, on the other hand, are in parallel in the suggested new design (Figure 2). They may share the load and thus minimize energy usage. Our study focused on the design modification of arm and bucket actuator configurations for this purpose since the main function of a boom actuator configuration is to hold the connected arm and bucket for stable excavation against gravity. The sizes of links for the fabricated prototype are presented in Table 1.

Table 1. The lengths of links in the proposed design prototype.

Link Name	Boom	Arm	Bucket
Link Size	100 cm	60 cm	40 cm

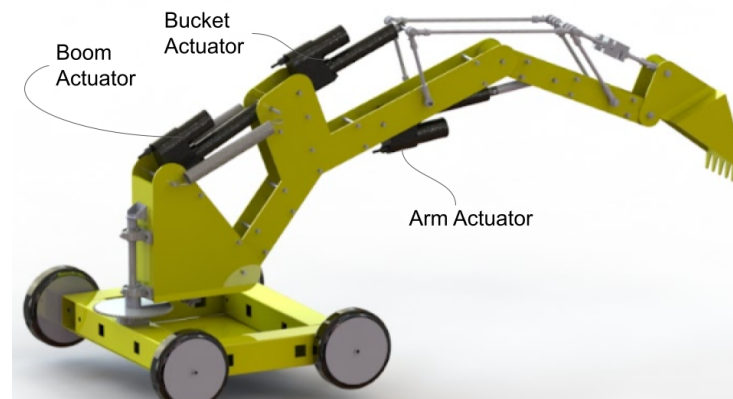
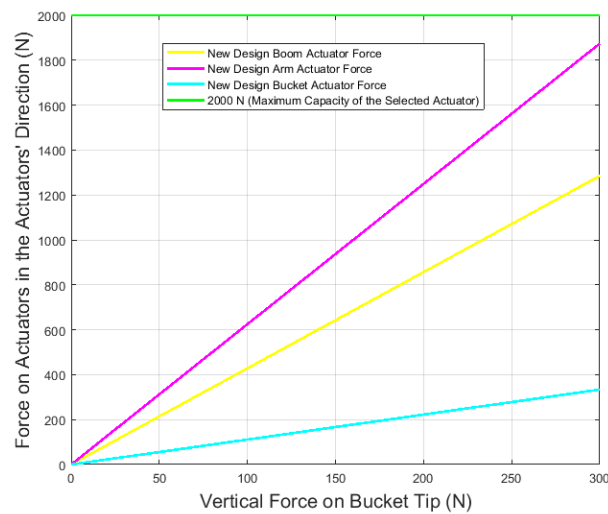


Figure 2. The proposed excavator design (the lengths of the boom, arm, and bucket links are 100 cm, 60 cm, and 40 cm, respectively) [24].

One notable distinction between the conventional excavators and this new design is the employment of two actuators operating in parallel. This arrangement facilitates load distribution between them. Unlike conventional excavators, where three actuators on their manipulators operate in series, our design has the arm and bucket actuators functioning simultaneously to evenly distribute the load [24].

This study proposes a novel design for an electric excavator utilizing linear lead screw actuators, leveraging their low back-drivability to conserve energy during idle periods and lower load capacity than hydraulic actuators. Specifically, the parallel arrangement of the linear actuators in the new design aims to decrease the load distribution on them [24].

The simulation results in Figure 3 indicate that the actuators in the new design do not encounter more than the acceptable load under a 300 N vertical load on the bucket tip, which is calculated based on the volume of the bucket. In the identical condition for the traditional design, however, the arm and boom actuators experience more than the permissible load (Figure 4).



**Figure 3.** The results of a load simulation on the new design (2000 N is the load capacity of the linear actuator selected for the prototype in this study).

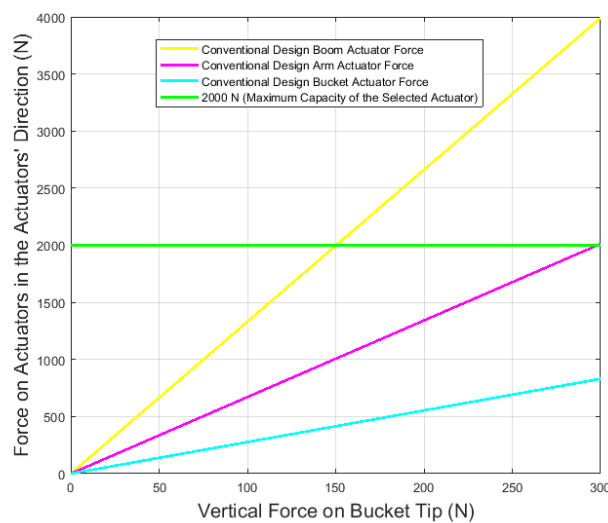


**Figure 4.** The results of a load simulation on the conventional design (2000 N is the load capacity of the linear actuator selected for the prototype in this study).

The proposed excavator and an indoor testbed, as shown in Figure 5, were fabricated in this study to evaluate the performance of the suggested trajectory development algorithms.



**Figure 5.** The fabricated excavator and the testbed.

The first three actuators mounted on the excavator are electric linear actuators (Figure 6) for the boom, arm, and bucket motions, while the fourth is a geared rotary DC motor for manipulating swing motion. A rotational DC electric motor is linked to a lead screw through a series of pulleys and a belt in the electric linear actuator. The motor is also linked to a rotary potentiometer, which provides feedback on the length of the actuator. In addition, the linear actuators in this excavator are connected to an electric grid as a power source.

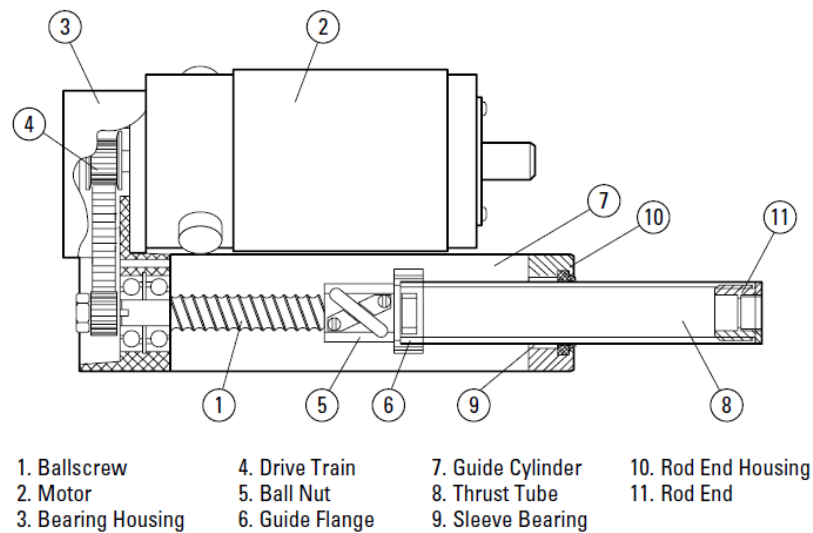


**Figure 6.** The components of the linear electric actuator [25].

The dynamic load capacity of the chosen linear actuators is 2000 N, and they all move at a speed of 20 mm/s. The boom link can be raised higher with the assistance of two enormous extension springs (Figure 7). These springs have a maximum force application of 70 kgf. The structure of the excavator was fabricated with laser-cut 2D sheets of aluminum and stainless steel. The boom and arm links of the excavator were made of aluminum and were assembled using M12 bolts (Figure 8).



**Figure 7.** Two massive springs helping the boom actuator raise the manipulator.



**Figure 8.** The arm link of the excavator.

By employing laser-cut metal sheets and M12 connecting bolts between the sheets, the aforementioned arrangement enables the power transmission links to be robust while being light and simple to produce. Welding was used in the production of the excavator's bucket and bottom frame. A swing mechanism was constructed utilizing a geared DC rotary motor, a set of pulleys, and a drive chain since the excavated material must be deposited on the right or left side of the excavator. The driving chain has a 1:5 reduction ratio (Figure 9), and the entire excavator revolves around a 25 mm diameter stainless steel shaft (Figure 10).



**Figure 9.** The drive chain for the swing motion.

A rotary potentiometer that is oriented with the rotation axis can also be used to gauge the rotation angle.

Four cut steel tubes were welded together with a steel sheet underneath to form the excavator's bottom frame (Figure 11). This structure has four nonactive wheels to facilitate its movement. The excavator's manipulator (Figure 12) was then mounted to the bottom framework utilizing two robust bearings.



**Figure 10.** Rotation axis and the associated rotary potentiometer.



**Figure 11.** The lower structure of the excavator.



**Figure 12.** The excavator's manipulator part.

For the indoor tests, the excavator was positioned at a height of 85 cm, and it was driven to remove a pile of sand from the main container and transfer it to the side container. The main container featured a transparent acrylic sheet that enabled comparisons between the actual path and the surface of the excavated earth at each dig. A RealSense depth camera [26], mounted at a distance from the main container's transparent side and linked to a PC, was used for monitoring the sand's profile in the container. The camera's sensory data were post-processed using MATLAB R2021a software [27]. The first step of post-processing was to capture and crop the data, and then, the sand's profile in the container considered as the ground shape was detected using the edge detection library in MATLAB. In the final step, the edge with the lowest height was selected as the ground edge. Using this method, the surface shape of the sand could be detected, as shown in Figure 13. Occasionally, when sand got stuck to the transparent acrylic sheet, the edges were manually trimmed.



**Figure 13.** Detecting ground shape using RGB camera and MATLAB R2021a software.

### 3. Methodologies for Path Generation and Tracking Control

#### 3.1. Path Generation

In addition to the use of parallel actuators that can save more energy by reducing the load on actuators, optimal path generation was also taken into consideration in this study to reduce the energy consumption of an autonomous excavator. For this purpose, the excavator bucket was viewed as a mobile robot that can move in 2D space and rotate around a single axis. These three DOFs (degrees of freedom) were controlled by the boom, arm, and bucket linear actuators. Figure 14 shows how the bucket and a mobile robot are comparable.

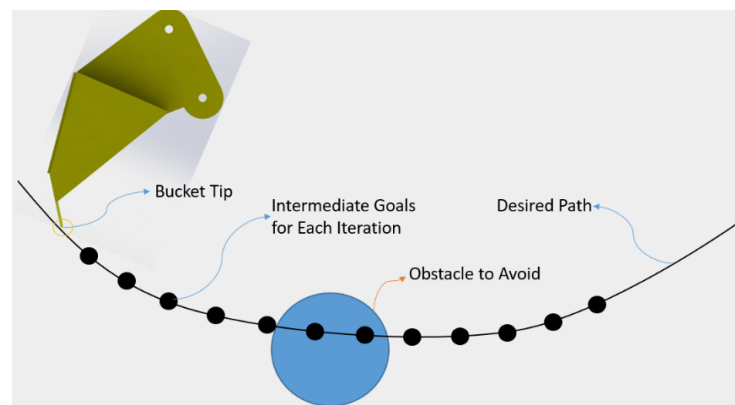


**Figure 14.** Similarities between the bucket and a mobile robot [24].

The obstacles can be pre-determined by the user or be detected using any real-time detection method. Various methods are available for detecting the presence and position of underground objects. Among them, Ground Penetration Radar (GPR) [28] and Electrical Resistivity Tomography (ERT) [29] have been widely recognized. However, these techniques are expensive and time consuming to implement and operate. An alternative study utilized cost-effective magnetic sensors affixed to the excavator bucket to detect and locate metal pipes and electricity-carrying wires based on their magnetic fields [30].

The excavator bucket moves along the designated route (i.e., path) while avoiding obstacles, like a mobile robot. However, to create an appropriate route for the reduction of energy consumption, energy conservation was included as a further component.

In this study, energy consumption was calculated using two methods. In the first method, energy can be calculated using Equation (1) for simulation scenarios:

$$Energy = \int_{t=0}^{t=T} F_1 \times V_1 + F_2 \times V_2 + F_3 \times V_3 dt \quad (1)$$

where  $V_1$ ,  $V_2$ , and  $V_3$  are the speeds of the boom, arm, and bucket actuators, respectively, and  $F_1$ ,  $F_2$ , and  $F_3$  are the calculated loads on each. Also,  $t$  represents the time, while  $T$  is the time at which the task is completed. In the second method, Equation (2) is used to calculate the energy consumption for actual excavator experiments:

$$Energy = \int_{t=0}^{t=T} Vol_1 \times I_1 + Vol_2 \times I_2 + Vol_3 \times I_3 dt \tag{2}$$

where  $Vol_1$ ,  $Vol_2$ , and  $Vol_3$  are the consumed voltages of the boom, arm, and bucket actuators, and  $I_1$ ,  $I_2$ , and  $I_3$  are the consumed electrical currents of each.

### 3.1.1. PSO-Based Path Generation

Particle swarm optimization (PSO) is a computational technique inspired by the collective behavior of animals like birds and fish. It is used to solve optimization problems by iteratively adjusting the positions and velocities of particles in a search space. PSO aims to find the best solution by balancing exploration and exploitation [19].

This study utilized the PSO algorithm to generate optimal pathways aimed at minimizing energy consumption during excavation while avoiding underground obstacles. The primary objectives were to reduce energy usage, reduce the deviation of the excavated ground shape of the desired profile, and increase the distance from underground objects. The algorithm endeavors to attain these objectives by minimizing the cost function specified in Equation (3). Throughout the optimization process, each iteration aims to identify parameters yielding the lowest possible value for the cost function:

$$Cost = W_1 \times GoalDistance + W_2 \times Energy + W_3 \times (1/ObjectDistance) \tag{3}$$

where  $W_1$ ,  $W_2$ , and  $W_3$  are the gains in this optimization problem that reflect the priority of each element to be optimized. These gains for the used system were obtained through trial and error. MATLAB simulation results show that the PSO-based optimization process with energy saving (Figure 15) can lower energy usage by 18.5% compared to the same process without energy saving (Figure 16), while attempting to avoid the subsurface obstruction and achieving a closer path to the desired ground shape.

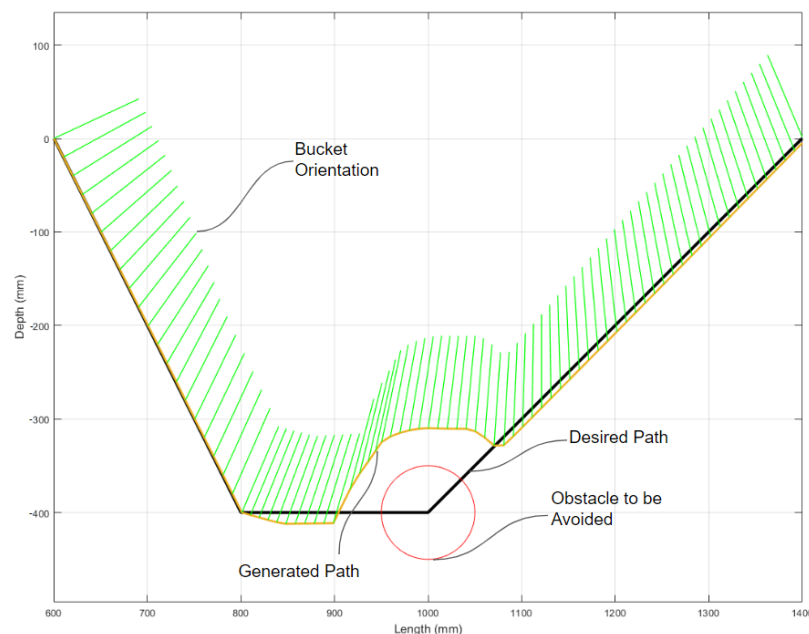


Figure 15. Path generation simulation while considering energy saving [24].

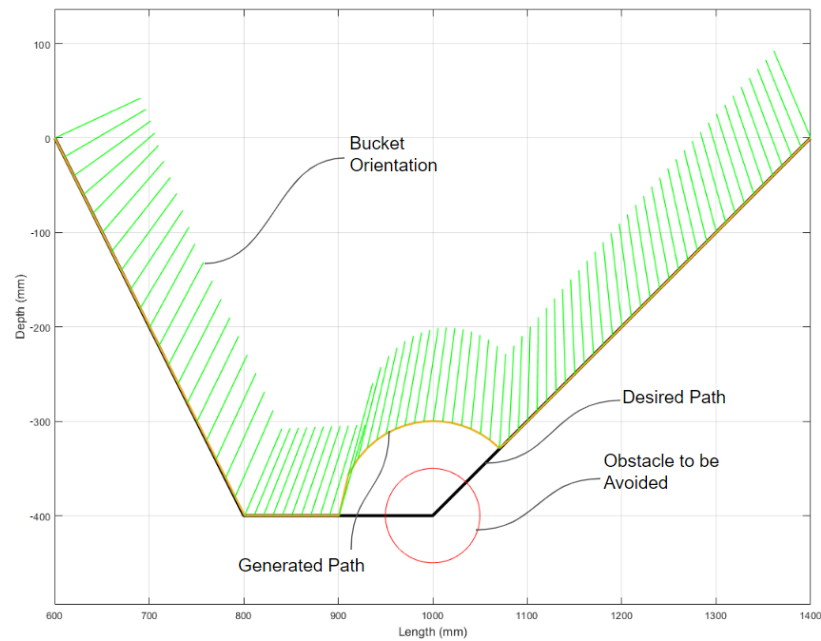


Figure 16. Path generation simulation without considering energy saving [24].

### 3.1.2. PFM-Based Path Generation

In the PFM algorithm, the environment is represented as a potential field in which a robot tries to reach the goal with the least possible potential. Consequently, a robot moves toward the neighboring locations with the least potential in each iteration, and it eventually finds an optimized path to the goal by traversing these locations. In the method, the goal generates negative and attractive potentials, whereas obstacles generate positive and repulsive potentials. Here, ‘potential’ is directly correlated with the cost function described in Equation (3).

The robot attempts to reach the target that pulls it in the PFM-based path planning (Figure 17). In contrast, an object that the robot is attempting to get away from pushes it away. The magnitude of the aforementioned pushing force vectors from the objects may vary depending on their size. Finally, the robot chooses the direction by summing these two vectors (force vectors initiated by the goal point and the object), and its speed is chosen based on the size of the total summed vector [31].

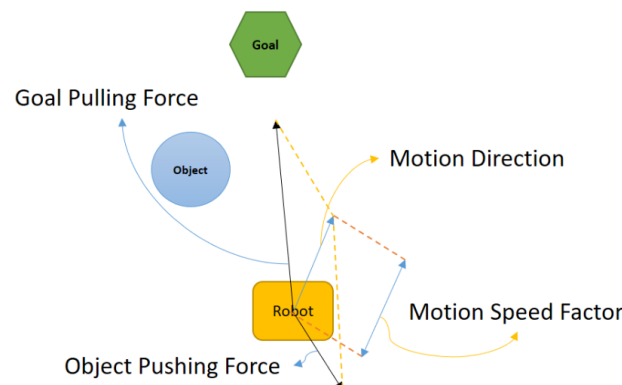
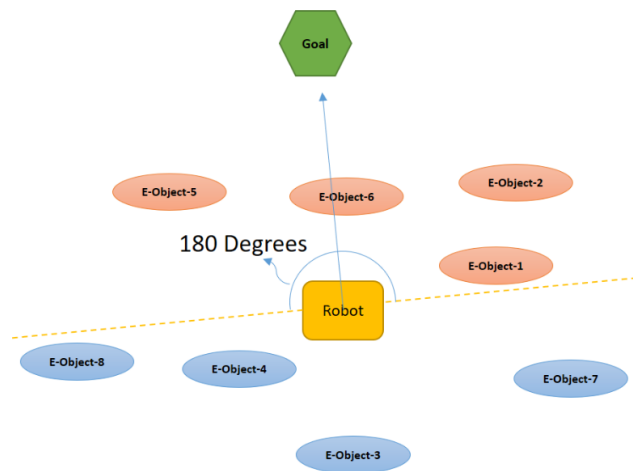


Figure 17. The principle of PFM.

To create a motion for energy saving, an artificial object was built that can pull the robot in a direction that consumes less energy. This artificial object is referred to as the E-Object in this study. This E-Object, however, should be placed in the area so that the robot’s movement toward it does not increase the distance between the robot and the

destination point (Figure 18). From several locations surrounding the robot, the E-Object will be chosen at the one that requires the least amount of energy to reach.



**Figure 18.** Candidate points for creating E-Objects that reduce energy consumption.

Figure 18 illustrates how the E-Objects that do not increase the distance between the robot and the goal point are selected. For reaching these E-Objects (shown with orange ovals in Figure 18) the robot does not need to get away from the goal point. In Figures 18 and 19, it is assumed that E-Object-2 consumes the least amount of energy among orange candidates.

To adhere to the PFM’s core idea of obstacles pushing the robot, an artificial energy object (A-E-Object-2) is produced on the opposite side of the robot at the same distance from it (Figure 19).

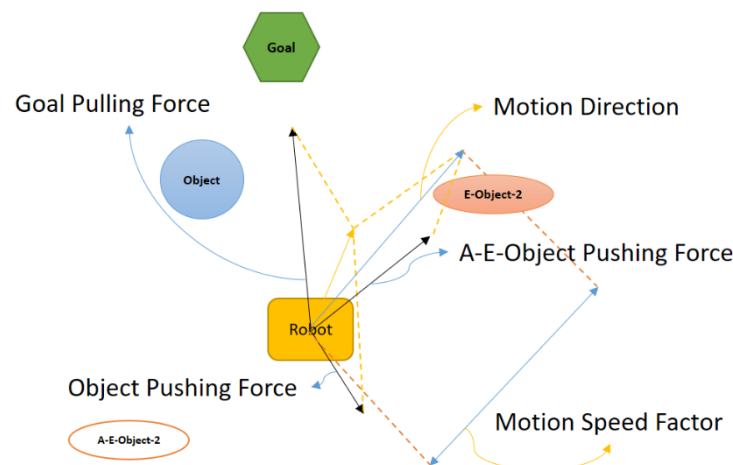


**Figure 19.** PFM with energy-saving.

The PFM algorithm will then determine the direction and magnitude of the robot’s speed, taking into account both real and artificial energy obstacles, as well as the target point.

In comparison to PSO, the PFM is generally less compatible with dynamic conditions. While PSO can adapt to changing conditions through the exploration and exploitation abilities of the particle swarm, PFM typically requires a static model for effective navigation.

During this study’s tests, sand was selected as a soil type, which exhibits fluid-like behavior due to its granular nature and lack of cohesive forces between individual grains. Therefore, sand grains can move fast with each other, resulting in a flow similar to a liquid when subjected to external forces such as gravity, vibrations, and shear forces.

Due to the aforementioned nature of the sand being excavated, it is difficult to determine the load on the bucket of the excavator accurately. Consequently, as the adjustment of parameters for the PFM algorithm is greatly influenced by system dynamics, the parameters tuned for simulating PFM were not aligned with those in real-world experiments. Hence, simulation results are omitted for PFM-based path generation.

### 3.2. Path Tracking Control

Path tracking is as critical as path generation. This is because the generated path should be tracked precisely to achieve the desired motion, which allows for consuming the least energy and has the least deviation between the followed and created paths. Two types of path tracking controllers were utilized and compared in this study to compel the excavator's bucket tip to follow the designed path.

#### 3.2.1. Proportional–Integral–Derivative (PID) Controller

The PID controller [32] was considered in this study since it has been widely used in industrial applications. This controller was employed to ensure that each actuator's stroke follows its required value. However, before regulating this stroke, the desired stroke for each actuator must be calculated based on the generated trajectory. For each sampling time, the created trajectory contains three components: the bucket's  $X$  and  $Z$  coordinates, as well as its orientation about the  $Y$  axis ( $Theta$ ). An inverse kinematic model [33] was used to convert this trajectory to the desired stroke for each actuator.

The required output signal (i.e., voltage) for the controller was then produced by computing the error between the actual and target stroke values for each actuator.

This controller's  $P$ ,  $I$ , and  $D$  gains were fine-tuned through trial and error. Each actuator's load exhibits different dynamic behavior, and therefore, distinct control gains were obtained. The controller's  $P$ ,  $I$ , and  $D$  gains were set to 100, 3, and 0.7 respectively.

#### 3.2.2. Contour Controller (CC)

The contour error ( $\epsilon$ ) is defined as the smallest distance between the bucket tip's actual current position of the excavator bucket tip and the planned reference trajectory (contour), as shown in Figure 20. To eliminate contour errors, the contour control approach was used to obtain the desired excavation surface.

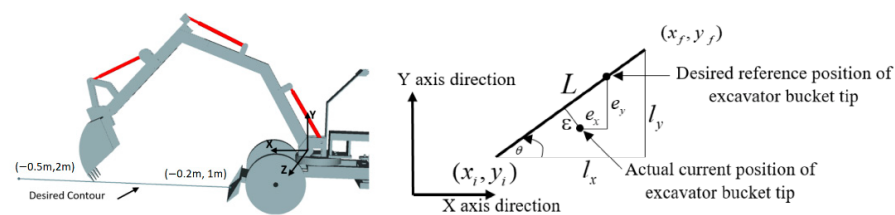


**Figure 20.** An example of the desired trajectory (contour) of the bucket tip (left) [34] and the contour error (right) [34].

There are three distinct components of the contour error, which include the error of the bucket tip's  $X$  position,  $Y$  position, and angle.

In the CC [34], the error between the bucket tip's desired and actual  $X$  and  $Y$  positions, as well as the error between its desired and real angles around the  $Z$  axis, are used as inputs to three distinct PID controllers (Figure 21). The outputs of these controllers are added to the desired values of  $X$ ,  $Y$ , and  $Theta$ . Then, these combined values become the input to the inverse kinematic block in the control system. In Figure 22, which shows the entire control design, the inverse kinematic output is sent to the PID controllers, which regulate the stroke of each actuator [35].

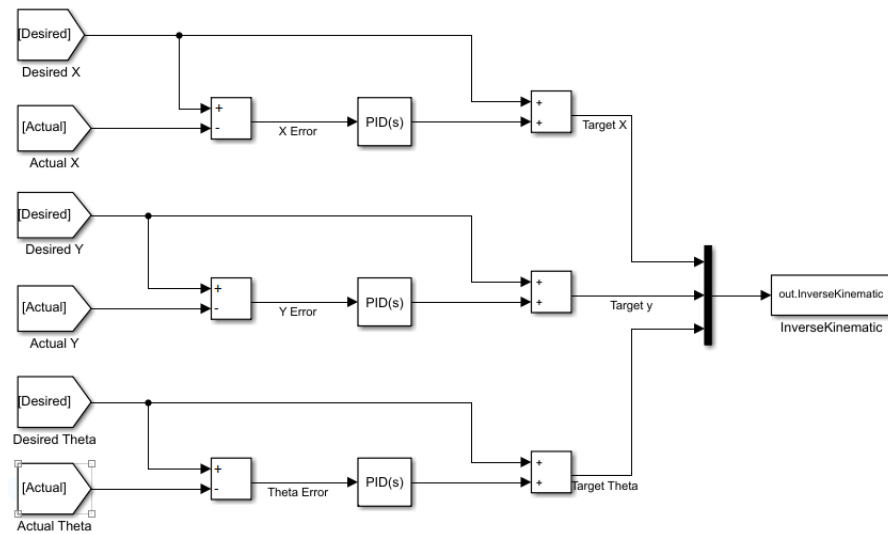


Figure 21. Contour controller working principle.

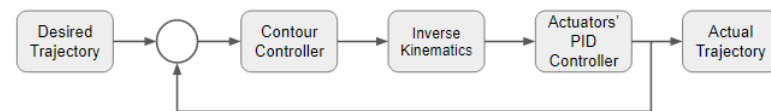


Figure 22. Block diagram of the entire control design.

#### 4. Experimental Results

To evaluate the capability of the proposed path generation techniques on avoiding obstacles, a 16 cm diameter pipe was buried, as illustrated in Figure 23.

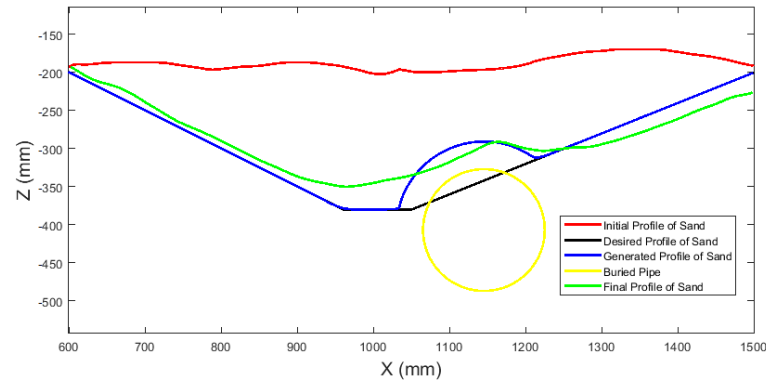


Figure 23. A pipe (white circle) was buried underground to perform the role of an underground obstacle.

Until the bucket is full of sand, the bucket tip follows the designed trajectory. The excavator then empties the sand into the side container after rotating. A user-specified desired profile was used to evaluate the suggested path generation algorithms. All PFM-based and PSO-based algorithms were applied to produce the pathways while taking into account the underground pipe. The camera was then used to detect the surface profile of the sand in the container and compare it to the original path.

Test results using the PSO algorithm are shown in Figures 24 (Scenario A) and 25 (Scenario B) without and with consideration for energy conservation. Figures 26 (Scenario C) and 27 (Scenario D) also show test results for the PFM algorithm without and with the energy conservation component. In each of these cases, the autonomous excavator followed the target trajectory with the aid of a PID controller. But in Figure 28 (Scenario E), combining the contour and PID controllers with the PFM-based trajectory generator enabled the

excavator to follow the target trajectory reasonably. The green line in each figure illustrates the contour of the earth when the digging procedure is complete. The desired digging profile and the original ground profile are indicated by the black and red lines, respectively. The yellow circle depicts the subterranean pipe, while the blue line shows the trajectory created by the path creation algorithm.



**Figure 24.** Test results for the PSO-based path generation without considering saving energy (Scenario A) and using a PID controller.

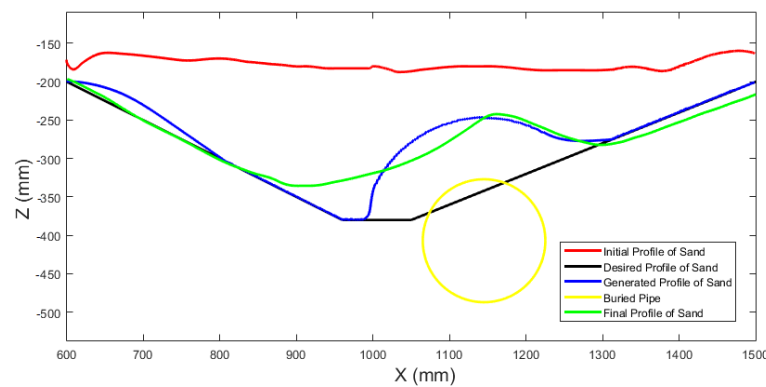


**Figure 25.** Test results for the PSO-based path generation considering saving energy (Scenario B) and using a PID controller.

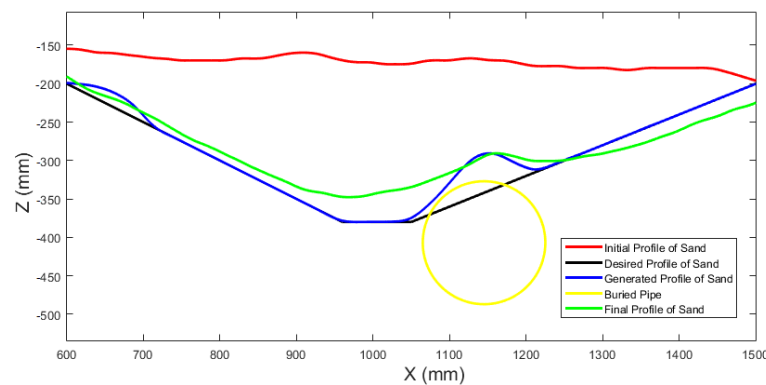


**Figure 26.** Test results for the PFM-based path generation without considering saving energy (Scenario C) and using a PID controller.

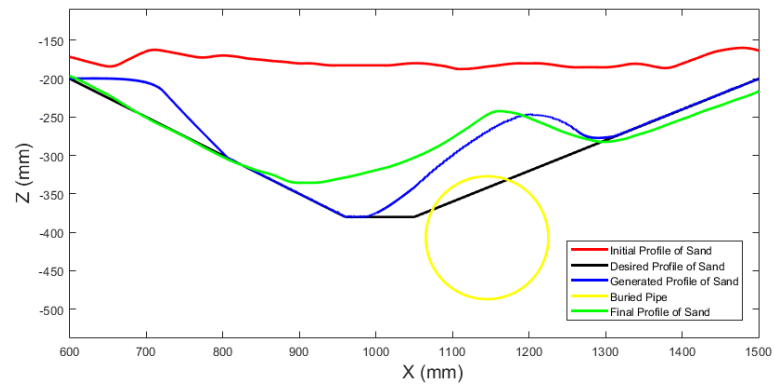


**Figure 27.** Test results for the PFM-based path generation considering saving energy (Scenario D) and using a PID controller only.

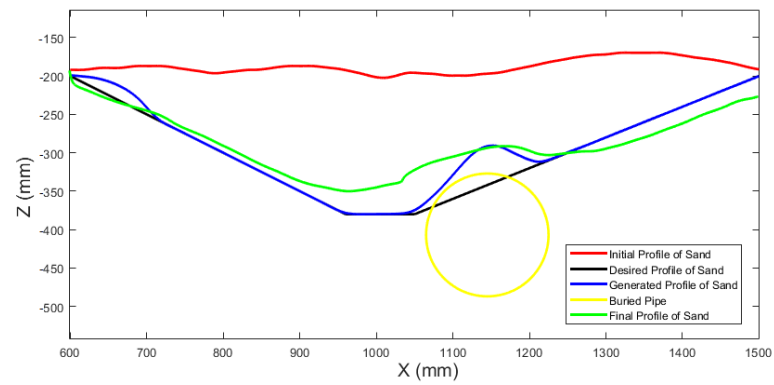


**Figure 28.** Test results for the PFM-based path generation considering saving energy (Scenario E) and using both contour and PID controllers.

In Figure 29, the average deviation between the designed profile and the final ground surface for Scenarios A, B, C, and D was between 15mm and 20mm, while it was about 12 mm for Scenario E.

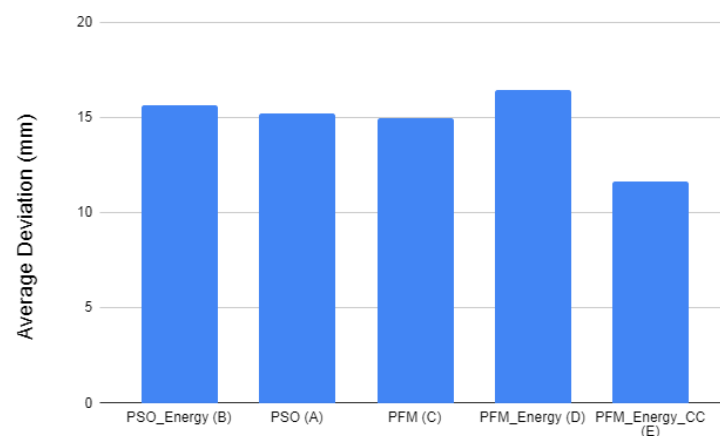


**Figure 29.** Path-following accuracy comparison between different scenarios.

The PFM-based trajectory generation algorithm, on the other hand, allowed the excavator to use less energy than the PSO-based path generation method, as seen in Figure 30. In addition, both techniques consume less energy when the energy-saving mode is engaged, as seen in Tables 2 and 3. However, the combination of the PID and contour controllers re-

quires higher control effort than the PID controller alone to give enhanced digging precision, and thus, this consumes more energy.

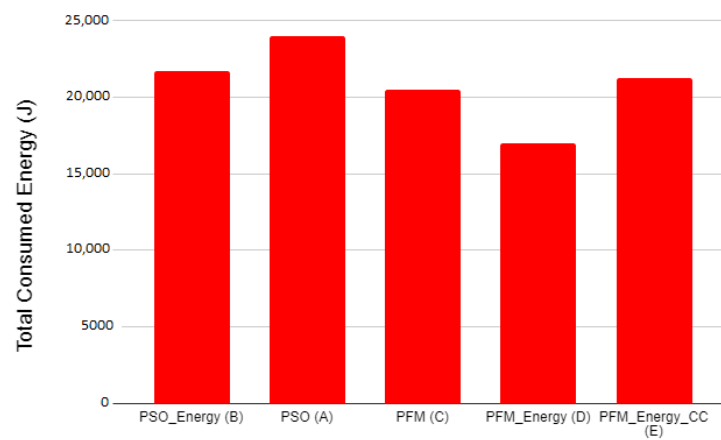


Figure 30. Energy consumption comparison between different scenarios.

Table 2. Energy consumption comparison between Scenarios A and B.

Scenario	A	B
Consumed Energy (KJ)	24.1	22.6
Energy Reduction Compared To Scenario A	N/A	6.22%

Table 3. Energy consumption comparison between Scenarios C, D and E.

Scenario	C	D	E
Consumed Energy (KJ)	20.7	16.9	21.3
Energy Reduction Compared To Scenario C	N/A	18.36%	−2.9%

### 5. Conclusions

A new design for manufacturing an electric autonomous excavator was proposed in this study, which uses two parallel actuators to distribute the load among them and lessen the stress placed on each of them. The designed electric excavator can apply greater force to the ground while consuming less energy. The proposed path generation approach employing the PSO and PFM algorithms was tested using the manufactured excavator. For this test, five separate scenarios were examined and compared based on the type of trajectory generator, the type of controller, and the state of the energy conservation mode.

For Scenario E (PFM-based trajectory generation with integrated contour and PID controllers), the smallest error between the designed profile and the final excavated surface occurs. This demonstrates that this control strategy is effective for an autonomous excavator to achieve a high excavation accuracy. On the other hand, the paths generated by the PFM algorithm require less energy than those with the PSO. If energy conservation in the PFM approach is taken into account, the amount of energy consumed can be significantly reduced. However, the contour controller plus PID controller uses more energy than the PID controller alone for the same proposed trajectory since it strives to maintain high precision and combines their control efforts.

As future work, several possible approaches can be applicable to solving the same topic. For example, Vector Field Histograms (VFHs) can be used to determine possible directions for navigation, avoiding obstacles while heading toward a goal based on the created polar histogram of the environment. ACO (Ant Colony Optimization) could also be a valuable candidate method, as explained in the introduction. Additionally, the developed algorithms were tested for sand excavation using an indoor setup only. This limitation

arises from the current excavator design, which lacks mobility and water resistance. Hence, it is imperative to incorporate active wheels and waterproof covers into the excavator's design for future deployment. This consideration will enable experiments with diverse materials such as silt, clay, and gravel in outdoor environments. Moreover, this study employed a camera a distance away from the sand container's transparent plate to monitor the ground profile, but this is impractical in an outdoor environment. Thus, an additional type of sensor such as Lidar will be required to deal with this issue and accurately measure the ground shape.

**Author Contributions:** Conceptualization, O.A.K. and J.S.; methodology, O.A.K. and J.S.; software, O.A.K.; validation, O.A.K. and J.S.; formal analysis, O.A.K. and J.S.; investigation, O.A.K. and J.S.; resources, O.A.K., J.S. and X.L.; data curation, O.A.K.; writing—original draft preparation, O.A.K.; writing—review and editing, O.A.K. and J.S.; visualization, O.A.K.; supervision, J.S.; project administration, J.S. and X.L.; funding acquisition, J.S. and X.L. All authors have read and agreed to the published version of the manuscript.

**Funding:** This research was supported by the Natural Sciences and Engineering Research Council of Canada (NSERC). Grant no: RGPIN-2020-05663.

**Institutional Review Board Statement:** Not applicable.

**Informed Consent Statement:** Not applicable.

**Data Availability Statement:** The datasets presented in this article are not readily available because of protecting confidential information. Requests to access the datasets should be directed to the corresponding author.

**Conflicts of Interest:** The authors declare no conflict of interest.

## Abbreviations

The following abbreviations are used in this manuscript:

PSO Particle Swarm Optimization;  
PFM Potential Field Method.

## References

- Malmgren, I. Quantifying the Societal Benefits of Electric Vehicles. *World Electr. Veh. J.* **2016**, *8*, 996–1007. [CrossRef]
- Perujo, A.; Ciuffo, B. The introduction of electric vehicles in the private fleet: Potential impact on the electric supply system and on the environment. A case study for the Province of Milan, Italy. *Energy Policy* **2010**, *38*, 4549–4561. [CrossRef]
- Bedotti, A.; Campanini, F.; Pastori, M.; Riccò, L.; Casoli, P. Energy saving solutions for a hydraulic excavator. *Energy Procedia* **2017**, *126*, 1099–1106. [CrossRef]
- Yang, J.; Quan, L.; Yang, Y. Excavator energy-saving efficiency based on diesel engine cylinder deactivation technology. *Chin. J. Mech. Eng.* **2012**, *25*, 897–904. [CrossRef]
- Ge, L.; Quan, L.; Zhang, X.; Dong, Z.; Yang, J. Power Matching and Energy Efficiency Improvement of Hydraulic Excavator Driven with Speed and Displacement Variable Power Source. *Chin. J. Mech. Eng.* **2019**, *32*, 100. [CrossRef]
- Quan, Z.; Quan, L.; Zhang, J. Review of energy efficient direct pump controlled cylinder electro-hydraulic technology. *Renew. Sustain. Energy Rev.* **2014**, *35*, 336–346. [CrossRef]
- Malafeev, S.I.; Novgorodov, A.A. Design and implementation of electric drives and control systems for mining excavators. *Russ. Electr. Eng.* **2016**, *87*, 560–565. [CrossRef]
- Kuznetsov, N.K.; Iov, I.A.; Iov, A.A. Reducing of dynamic loads of excavator actuators. *J. Phys. Conf. Ser.* **2019**, *1210*, 012075. [CrossRef]
- Volvo CE Unveils 100% Electric Compact Excavator Prototype. Available online: <https://www.volvoce.com/global/en/news-and-events/news-and-stories/2017/volvo-ce-unveils-100-percent-electric-compact-excavator-prototype/> (accessed on 10 July 2022).
- Lucidarme, P.; Delanoue, N.; Mercier, F.; Aoustin, Y.; Chevallereau, C.; Wenger, P. Preliminary Survey of Backdrivable Linear Actuators for Humanoid Robots. *CISM Int. Cent. Mech. Sci. Courses Lect.* **2019**, *584*, 304–313. [CrossRef]
- Dietrich, A. Electric rod actuators vs. hydraulic cylinders A comparison of the pros and cons of each technology. *Mach. Des.* **2016**, 1–13.
- Bae, J.; Lee, C.S.; Hong, D. Avoidance of earth obstacles for intelligent excavator. In Proceedings of the 28th International Symposium on Automation and Robotics in Construction, ISARC 2011, Seoul, Republic of Korea, 29 June–1 July 2011; pp. 1184–1189. [CrossRef]

13. Katsuma, S.; Yajima, R.; Hamasaki, S.; Chun, P.J.; Nagatani, K.; Yamauchi, G.; Hashimoto, T.; Yamashita, A.; Asama, H. Excavation Path Generation for Autonomous Excavator Considering Bulking Factor of Soil. In Proceedings of the 37th International Symposium on Automation and Robotics in Construction, ISARC 2020: From Demonstration to Practical Use—To New Stage of Construction Robot, Kitakyushu, Japan, 26–30 October 2020; pp. 578–583. [CrossRef]
14. Yang, Y.; Pan, J.; Long, P.; Song, X.; Zhang, L. Time Variable Minimum Torque Trajectory Optimization for Autonomous Excavator. *arXiv* **2020**, arXiv:2006.00811. <https://doi.org/10.48550/arxiv.2006.00811>.
15. Zhao, J.; Hu, Y.; Liu, C.; Tian, M.; Xia, X. Spline-Based Optimal Trajectory Generation for Autonomous Excavator. *Machines* **2022**, *10*, 538. [CrossRef]
16. Sandzimier, R.J.; Asada, H.H. A Data-Driven Approach to Prediction and Optimal Bucket-Filling Control for Autonomous Excavators. *IEEE Robot. Autom. Lett.* **2020**, *5*, 2682–2689. [CrossRef]
17. Wind, H.; Renner, A.; Bender, F.A.; Sawodny, O. Trajectory generation for a hydraulic mini excavator using nonlinear model predictive control. In Proceedings of the IEEE International Conference on Industrial Technology, Buenos Aires, Argentina, 26–28 February 2020; pp. 107–112. [CrossRef]
18. Srivastava, P.R.; Baby, K.; Raghurama, G. An approach of optimal path generation using ant colony optimization. In Proceedings of the IEEE Region 10 Annual International Conference, Proceedings/TENCON, Singapore, 23–26 January 2009. [CrossRef]
19. Deepak, B.B.; Parhi, D.R. PSO based path planner of an autonomous mobile robot. *Open Comput. Sci.* **2012**, *2*, 152–168. [CrossRef]
20. Wang, Y.; Chirikjian, G.S. A New potential field method for robot path planning. In Proceedings of the IEEE International Conference on Robotics and Automation, San Francisco, CA, USA, 24–28 April 2000; Volume 2, pp. 977–982. [CrossRef]
21. Luo, L.; Wen, H.; Lu, Q.; Huang, H.; Chen, W.; Zou, X.; Wang, C. Collision-free path-planning for six-DOF serial harvesting robot based on energy optimal and artificial potential field. *Complexity* **2018**, *2018*, 3563846. [CrossRef]
22. Szczepanski, R.; Tarczewski, T.; Erwinski, K. Energy Efficient Local Path Planning Algorithm Based on Predictive Artificial Potential Field. *IEEE Access* **2022**, *10*, 39729–39742. [CrossRef]
23. Products & Services—North America | Cat | Caterpillar. Available online: <https://www.cat.com/en-US.html> (accessed on 10 August 2022).
24. Khiyavi, O.A.; Seo, J.; Lin, X. Energy Saving in an Autonomous Excavator via Parallel Actuators Design and PSO-Based Excavation Path Generation. *Eng. Proc.* **2022**, *24*, 5. [CrossRef]
25. Types of Linear Actuators | Kollmorgen. Available online: <https://www.kollmorgen.com/en-us/blogs/types-of-linear-actuators> (accessed on 15 August 2022).
26. Depth Camera D455—Intel® RealSense™ Depth and Tracking Cameras. Available online: <https://www.intelrealsense.com/depth-camera-d455/> (accessed on 6 June 2022).
27. MATLAB-MathWorks-MATLAB and Simulink. Available online: <https://www.mathworks.com/products/new-products/release-2021a> (accessed on 1 June 2022).
28. Saarenketo, T.; Scullion, T. Road evaluation with ground penetrating radar. *J. Appl. Geophys.* **2000**, *43*, 119–138. [CrossRef]
29. Perrone, A.; Lapenna, V.; Piscitelli, S. Electrical resistivity tomography technique for landslide investigation: A review. *Earth-Sci. Rev.* **2014**, *135*, 65–82. [CrossRef]
30. Khiyavi, O.A.; Seo, J.; Lin, X. Three-Dimensional Metal Pipe Detection for Autonomous Excavators Using Inexpensive Magnetometer Sensors. *IEEE Sens. J.* **2023**, *23*, 24383–24392. [CrossRef]
31. Koren, Y.; Borenstein, J. Potential field methods and their inherent limitations for mobile robot navigation. In Proceedings of the IEEE Conference on Robotics and Automation, Sacramento, California, 7–12 April 1991; Volume 2, pp. 1398–1404.
32. Ang, K.H.; Chong, G.; Li, Y. PID control system analysis, design, and technology. *IEEE Trans. Control Syst. Technol.* **2005**, *13*, 559–576. [CrossRef]
33. D’Souza, A.; Vijayakumar, S.; Schaal, S. Learning inverse kinematics. *IEEE Int. Conf. Intell. Robot. Syst.* **2001**, *1*, 298–303. [CrossRef]
34. Sheikha, F.H.; Afzalghaeinaeini, A.; Seo, J. Collaborative Tracking Control Strategy for Autonomous Excavation of a Hydraulic Excavator. *Eng. Proc.* **2021**, *10*, 43. [CrossRef]
35. Reginald, N.; Seo, J.; Cha, M. Integrative Tracking Control Strategy for Robotic Excavation. *Int. J. Control Autom. Syst.* **2021**, *19*, 3435–3450. [CrossRef]

**Disclaimer/Publisher’s Note:** The statements, opinions and data contained in all publications are solely those of the individual author(s) and contributor(s) and not of MDPI and/or the editor(s). MDPI and/or the editor(s) disclaim responsibility for any injury to people or property resulting from any ideas, methods, instructions or products referred to in the content.